IEEE Access
Multidisciplinary | Rapid Review | Open Access Journal

Received August 16, 2020, accepted September 6, 2020, date of publication September 18, 2020, date of current version October 12, 2020.

Digital Object Identifier 10.1109/ACCESS.2020.3024799

An Adaptive Control Method for Improving Voltage and Frequency Stability of Wind-Thermal Bundled System

XINYU LIU[1], CANBING LI[2], (Senior Member, IEEE), MOHAMMAD SHAHIDEHPOUR[3], (Life Fellow, IEEE), XINYAN LU[1], AND DI ZHANG[4], (Student Member, IEEE)

[1]School of Electric Power, North China University of Water Resources and Electric Power, Zhengzhou 450011, China
[2]Department of Electrical Engineering, Shanghai Jiao Tong University, Shanghai 200240, China
[3]Department of Electrical and Computer Engineering, Illinois Institute of Technology, Chicago, IL 60616, USA
[4]Department of Electrical and Information Engineering, Hunan University, Hunan 410082, China

Corresponding author: Xinyu Liu (lxy22101@163.com)

This work was supported in part by the Henan Science and Technology Research Project under Grant 162102210078, in part by the Henan Key Youth Teacher Research Project under Grant 2016GGJS-074, and in part by the Henan Provincial Department of Education Science and Technology Research Key Project under Grant 14B413005.

ABSTRACT Aiming at the low frequency oscillation and voltage drop caused by the wind-thermal bundled system transmitted to the load center across AC and DC lines, an adaptive sliding mode gain control method based on the structure decentralized control theory is proposed. On the basis of this method, a rotor-side adaptive terminal sliding mode controller for doubly-fed induction generator based on synchronous rotating coordinate system is designed. Based on RTDS, a real-time simulation platform for transient stability control of ''wind-thermal bundled'' transmission system was developed, and real-time simulation experiments were performed. Experimental results prove that the proposed method in this paper can effectively suppresses the frequency and voltage fluctuations of the system, significantly improve the transient stability of the system and enhance the robustness of the system during grid faults.

INDEX TERMS Wind-thermal bundled system, transient stability, adaptive control, sliding mode variable structure controller.

I. INTRODUCTION

When wind energy resources are concentrated in remote areas far away from the power load center, wind power cannot be integrated well. The large-scale wind power can be transmitted to the remote load center area through long-distance AC and DC transmission lines. However, When the output of the wind farm is reduced, this single wind power transmission mode causes a lower utilization rate of the transmission channel. In addition, when there is no other AC connection line, the wind-thermal bundled power transmission mode belongs to the island operation mode. When the AC system is disturbed in this mode, the usual constant power or constant current control method is likely to cause a continuous imbalance in the system power, which in turn leads to the destruction of the stable operation of AC and DC systems. And with the increasing scale of wind farms, the transmission capacity of the original AC lines that transmit wind energy gradually cannot meet the grid-connected requirements of wind farms. Therefore, it is possible to use the AC-DC parallel-connected transmission line based on VSC-HVDC to transmit power [2], which will be the most common operation mode for wind-thermal bundled power transmission in the future. In this way, the characteristics of conventional thermal power stations that can regulate frequency and voltage can be fully utilized, and the fluctuation of output power of the wind farm can be effectively mitigated.

Voltage source converter based on high voltage direct current transmission (VSC-HVDC) is a referable option to transmit wind power, which has become a hot topic [3]. Currently, there are some VSC-HVDC grid-connected wind farm projects around the world, such as Nanhui Project, Guangdong Nan'ao Flexible Project, Zhejiang Zhoushan Five-end Flexible Project, Sweden Gotland Project, Danish Tjareborg Project, Germany Nord E. ON 1 project and DolWin1 project. As for the wind-thermal bundled system, on the one hand,

The associate editor coordinating the review of this manuscript and approving it for publication was Huai-Zhi Wang.

due to the ''mechanical-electrolytic coupling'' characteristic of DFIG, its mechanical and electrical quantities are decoupled from each other, which makes it impossible to provide mechanical inertia for the power grid. Therefore, under the condition that the electric power at the DC transmitting end cannot be adjusted in time, when the system is disturbed, the adjustment burden of the thermal power unit will be increased. This feature of DFIG reduces the equivalent mechanical inertia of wind-thermal bundled power supplies, thereby weakening the system's ability to resist disturbances and reducing system stability. On the other hand, most wind farms in wind-thermal bundled systems are in remote areas, which are far away from power system, and the equivalent reactance is larger than the equivalent reactance which is near the load center. Therefore, the grid connected to the wind-thermal bundled power supply is a weak grid, and the grid is relatively weaker than the traditional power system [4]. Its transient stability and power quality are facing new challenges, such as transient voltage stability and frequency stability of the system after the wind farm is connected to the grid.

Some progress has been made in suppressing voltage fluctuations and damping power oscillations [5]–[7] for the transient stability of wind-thermal bundled system with AC-DC transmission. Reference [6] studied the power angle transient characteristics of the system under different wind power ratios and different DC control methods, and explored the interaction between wind power, thermal power and DC systems. It is believed that under the premise that the receiving end grid is an infinite system, increasing the proportion of wind power can improve the system's transient stability. Reference [8] analyzed the differences in the transient characteristics of wind turbines and thermal turbines and their respective effects on the transient stability of the system. An optimal control strategy for the generator tripping of the wind-thermal bundled system is proposed, and a calculation method for the control amount of the generator tripping is given. Reference [9] introduced the PSS (power system stabilization) control link to improve the damping of the DFIG (double fed induction generator) grid-connected system, and improved the ability of double-fed wind farms to suppress small disturbances in the power system. In addition, many scholars have adopted different control methods in order to achieve the goal of improving or increasing the transient stability of the system [10]–[13], such as increasing the reactive power output capability of DFIG to improve the transient stability of the system with small interference power angle; Improve the transient stability of the system by perfecting the system topology and operation mode; improve the transient stability of the wind and fire bundling system by adopting the correct cutting machine control strategy; increase the deceleration area of the synchronous machine by DC power boost to improve the system transient State stability, etc.

The previous literature has made preliminary explorations on the method and mechanism of rapid power regulation of wind and fire bundling transmission system, and has made some progress. At present, in an AC-DC parallel system, the active power transmitted by AC line and DC line is determined by the active power command value issued by the superior dispatching department, and the dispatching control time is usually minutes or even longer. However, the regulation of active power and reactive power of doubly fed wind farm during transmission system fault is a fast control at millisecond level, which is also the key to improve the quality of transmission system transient characteristics. Based on the grid-connected operation model of the wind-fire bundling AC / DC transmission system, this paper proposes a variable gain sliding mode additional control strategy for the rotor flux linkage of the doubly-fed wind power generator set to improve the transient stability of the grid-connected voltage and frequency of the doubly-fed wind farm. Based on the grid-connected operation model of wind-fired AC/DC transmission system, this paper studies and analyzes the ability of the double-fed wind farm itself to quickly and independently emit active and reactive power and its mechanism. A variable gain sliding mode variable structure adaptive control strategy for the doubly-fed wind turbine generator rotor magnetic chain is proposed to improve the transient stability of grid-connected voltage and frequency of doubly-fed wind farms.

The rest of the paper is organized as the follows. In Section II, the feasibility of rapid power adjustment is analyzed. In Section III, the DFIG flux adaptive sliding mode gain controller is designed. In Section IV, in order to verify the feasibility of the ''magnetic chain adaptive control'', a real-time simulation system of ''magnetic chain adaptive control'' based on RTDS was developed. In Section V, the conclusion is made.

II. RAPIDITY ANALYSIS OF DFIG DYNAMIC POWER REGULATION

In order to facilitate the research, the d-axis of the stator voltage vector is positioned in the direction of the grid voltage vector, because the stator resistance value is generally much smaller than the stator reactance value, the voltage drop on the stator resistance is ignored here.

In addition, when the stator voltage fluctuates due to a sudden change in the DFIG power angle, the DFIG stator flux linkage and stator voltage will not remain constant. Therefore, it is necessary to consider the influence of stator flux changes on DFIG grid connected operation.

It can be seen from [14] that the output power of the double-fed stator and the control equation of the rotor flux linkage can be expressed as follows:

$$\begin{cases} P_s = \dfrac{u_s L_m}{L_s} i_{qr} \\ \quad = \dfrac{u_s L_m}{L_m^2 - L_r L_s} \varphi_{qr} \\ Q_s = \dfrac{u_s L_m}{L_s} i_{dr} - \dfrac{u_s}{L_s} \varphi_{ds} \\ \quad = \dfrac{u_s L_m}{L_m^2 - L_r L_s} \varphi_{dr} + \dfrac{(L_m^2 - L_s L_m + L_r L_s^2) u_s}{L_s (L_m^2 - L_r L_s)} \varphi_{ds} \end{cases} \tag{1}$$

$$\begin{cases} \dot{\psi}_{dr} = \frac{1}{\tau}\psi_{dr} + \omega_s\psi_{qr} - \frac{L_m R_r}{L_s L_r - L_m^2}\dot{\Psi}_{qs} \\ \dot{\psi}_{qr} = \frac{1}{\tau}\psi_{qr} - \omega_s\psi_{dr} - \frac{R_r L_m U_g}{\omega_1(L_s L_r - L_m^2)} \\ \qquad + \frac{R_r L_m}{\omega_1(L_s L_r - L_m^2)}\dot{\Psi}_{ds} + u_{qr} \end{cases} \tag{2}$$

Among them, $\tau = \frac{L_s L_r - L_{mr}^2}{L_s R}$.

According to Equation (1), it can be seen that by controlling the magnetic flux of the DFIG rotor, it is possible to control the output active and reactive power of the stator. It can be seen from equation (2) that the flux of DFIG rotor flux depends on the control voltages and. The control time constant of doubly-fed wind farm transient power is, which value is generally 8 $\sim$ 15ms. Therefore, the speed of the doubly-fed wind farm's transient power regulation meets the requirements of millisecond-level rapid regulation. In addition, when the wind farm is connected to a weak grid, the transient power generated by the fast-adjusting wind farm will not significantly increase the rotor excitation current, and also will not bring adaptive burden on the inverter.

III. DESIGN OF DFIG ADAPATIVE ROTOR FLUX CONTROLLER

The electromechanical oscillation of the power system is caused by the unbalanced torque on the rotor of the synchronous generator. Some methods of generating adaptive electrical torque were proposed to damp electromechanical oscillations [15]. The method of damping system oscillation and increasing system transient voltage stability by using active power and reactive power generated by wind farm has been widely used by scholars [16]–[19]. The control strategy proposed in this paper satisfies the requirements of the following projects: firstly, the wind farm can send out transient power quickly, and secondly, the rotor will not have a negative impact on the inverter when the wind farm sends out transient power.

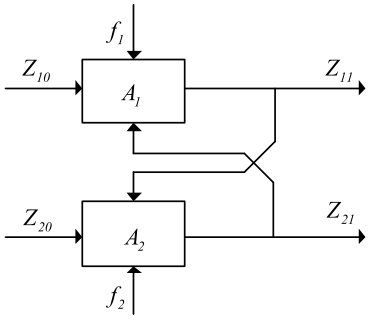

FIGURE 1. Decentralized model of flux structure for DFIG grid connected operation.

Figure 1 shows the decentralized model of the DFIG grid-connected magnetic chain structure.

It can be seen from Fig. 1 that the decentralized model of flux structure for DFIG grid connected operation includes two subsystems A_i. Z_{10} and Z_{20} represent control inputs, which respectively represent the excitation control voltage u_{dr} and the excitation control voltage u_{qr}. Z_{11} and Z_{21} represent controlled outputs, respectively representing the magnetic flux component ψ_{dr} and the magnetic flux component ψ_{qr}, which have mutual influences. As can be seen from the figure, the control amount Z_{i0} issued by the controller affects the controlled amount Z_{i1} by controlling the corresponding subsystem A_i. In this way, it is possible to design corresponding rotor flux controllers for the subsystem A_i to achieve control of the DFIG rotor flux.

In order to make the rotor flux-linkage controller have adaptive anti-interference ability in the event of power grid failure, a sliding mode variable structure controller can be designed to achieve this control goal. Therefore, equation (2) is organized into the form of a state space equation,

$$\dot{Z} = AZ + BU + F \tag{3}$$

where

$$A = \begin{bmatrix} -\frac{L_s R_r}{L_s L_r - L_m^2} & \omega_s \\ -\frac{L_s R_r}{L_s L_r - L_m^2} & -\omega_s \end{bmatrix}, \quad B = \begin{bmatrix} 1 & 0 \\ 0 & 1 \end{bmatrix},$$

$$F = \begin{bmatrix} f_1 \\ f_2 \end{bmatrix}, \quad f_1 = -\frac{L_m R_r}{L_s L_r - L_m^2}\dot{\Psi}_{qs},$$

$$f_2 = \frac{R_r L_m}{\omega_1(L_s L_r - L_m^2)}\dot{\Psi}_{ds} - \frac{R_r L_m u_g}{\omega_1(L_s L_r - L_m^2)},$$

F represents generalized perturbation, $Z = \begin{bmatrix} z_{11} \\ z_{21} \end{bmatrix}$ represents state variable, and $U = \begin{bmatrix} z_{10} \\ z_{20} \end{bmatrix}$ represents control input.

It can be known from equation (3),

$$rank\begin{bmatrix} B & F \end{bmatrix} = rank\,[B] = 2 \tag{4}$$

From Equation (4), it can be known that the sliding mode of the DFIG magnetic flux control system satisfies the necessary and sufficient conditions of being free from external interference. Here, the controller is only designed based on the relationship between the d-axis rotor current and the rotor voltage after grid connection. Other controllers can be designed accordingly. Suppose the current tracking error of the rotor d-axis $e_{\mathrm{dr}} = z_{11}^* - z_{11}$, where z_{11}^* represents a given value of the flux component ψ_{dr}, then the state equation of the d-axis flux tracking error of DFIG is that,

$$\dot{e_{dr}} = \omega_s z_{11}^* - \omega_s e_{dr} - z_{10} + z_{11}^* + F_{dr} \tag{5}$$

where is the disturbance caused by external disturbance and parameter change of the system. And

$$F_{dr} = \frac{L_s R_r - \omega_s L_s L_r + \omega_s L_m^2}{L_s L_r - L_m^2} z_{21} + \omega_s z_{11} - f_2.$$

In order to eliminate steady state errors and improve the robustness of the control system, an integral terminal sliding mode surface is adopted here,

$$s_{dr} = e_{dr} + \int_0^t (c_{1d} e_{dr} + c_{2d} e_{dr}^{p/q}) d\tau \tag{6}$$

In the equation (6), c_{1d} and c_{2d} are sliding surface parameters, which are greater than zero. p and q are odd numbers, which satisfy the relationship $q < p < 2q$.

A. EQUIVALENT CONTROLLER DESIGN

When the system enters the designed sliding surface, s_{dr} and s_{dr} are zero, then the following equation can be obtained,

$$\dot{e_{dr}} = -c_{1d}e_{dr} - c_{2d}e_{dr}^{p/q} \tag{7}$$

The state equation of system current error as follows,

$$\dot{e_{dr}} = \omega_s\Psi_{dr}^* - \omega_s e_{dr} - u_{dr} + \dot{\Psi}_{dr^*} + F_{dr} \tag{8}$$

By combining (7) and (8), the equivalent controller can be obtained,

$$u_{dreq} = (c_{1d}L_r - \omega_s)e_{dr} + L_r c_{2d}e_{dr}^{p/q} + \omega_s\psi_{dr}^* + \dot{\Psi}_{dr^*} + F_{dr} \tag{9}$$

B. SWITCH CONTROLLER DESIGN

Introduce switching controller here as follows,

$$u_{drn} = L_r\eta_d'\mathrm{sgn}(s_{dr}) \tag{10}$$

$$\eta_d' = (1 + \mu(s)e_d^{\lambda_d\mu(s)t})\eta_d \tag{11}$$

Among them $\mu(s_d) = \mathrm{sgn}(s_d)\mathrm{sgn}(s_d')$, $s_d'(t) = s_d(t + \tau')$, $0 < \lambda_d < 1$, τ' is the delay constant.

It can be seen from equation (10), since η_d' can be changed with the change of the motion state of the system, the value of the shake amplitude when the system makes a crossing motion near the sliding surface is small.

According to formula (9) and equation (10), the expression of the d-axis flux linkage controller is as follows,

$$\begin{aligned} u_{\Psi dr} &= u_{dreq} + u_{drn} \\ &= (c_{1d}L_r - \omega_s)e_{dr} + L_r c_{2d}e_{dr}^{p/q} + \omega_s\psi_{dr}^* \\ &\quad + \dot{\psi}_{dr}^* + F_{dr} + L_r\eta_d'\mathrm{sgn}(s_{dr}) \end{aligned} \tag{12}$$

Taking Lyapunov's function as $V = \frac{1}{2}s_{dr}^2$, then,

$$\begin{aligned} \dot{V} &= s_{dr} * \dot{s_{dr}} \\ &= s_{dr}(\dot{e_{dr}} + c_{1d}e_{dr} + c_{2d}e_{dr}^{p/q}) \\ &= s_{dr}(-\frac{R_r}{L_r}e_{dr} - \frac{1}{L_r}u_{dr} - F_{dr} + \dot{i_{dr}^*} \\ &\quad + \frac{R_r}{L_r}i_{dr}^* + c_{1d}e_{dr} + c_{2d}e_{dr}^{p/q}) \\ &= s_{dr}(-\eta_d\mathrm{sgn}(s_d) - F_{dr}) \\ &\le -\eta_d\,|s_{dr}| + |F_{dr}|\,|s_{dr}| \\ &= (|F_{dr}| - \eta_d')\,|s_{dr}| \\ &\le -\,|s_{dr}|\,(\eta_d' - k_d) \end{aligned} \tag{13}$$

Since the upper bound $k_d (k_d > 0)$ of the uncertainty F_d is unknown, there are two cases of the initial value of the switching gain η_d': One case is $\eta_d' > k_d$ and the other is $\eta_d' < k_d$. In the second case, due to η_d' can be changed, although the situation of $\eta_d' < k_d$ may appear temporarily, the value of the adaptive switching gain η_d' increases rapidly according to the designed control strategy, and finally makes $\eta_d' < k_d$, then, $\dot{V} \le -\,|s_{dr}|\,(\eta_d' - k_d) < 0$.

And because $V > 0$, the integral sliding mode variable structure controller designed in this paper is progressively stable over a wide range.

Similarly, we can get the q-axis flux controller expression as follows,

$$\begin{aligned} u_{\Psi qr} &= u_{qreq} + u_{qrn} \\ &= (c_{1q}L_r - \omega_s)e_{qr} + L_r c_{2q}e_{qr}^{p/q} + \omega_s\psi_{qr}^* \\ &\quad + \dot{\psi}_{qr}^* + F_{qr} + L_r\eta_q'\mathrm{sgn}(s_{qr}) \end{aligned} \tag{14}$$

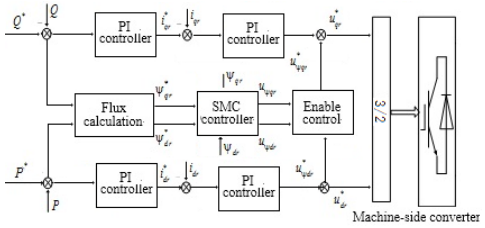

FIGURE 2. Block diagram of the adaptive control of the DFIG rotor flux linkage terminal sliding mode.

Based on the adaptive control rate designed above, the block diagram of the sliding mode control of the rotor flux linkage terminal of the doubly-fed induction wind turbine connected to the grid is shown in Figure 2. The function of the enable control link in the figure is that only when the power grid fails and the DFIG rotor magnetic flux changes drastically, the adaptive control generated by the magnetic chain sliding mode controller will work, and the adaptive control will not work when the system is in normal operation. The function expression used in the enable control link is as follows,

$$\begin{cases} u_{\psi dr}^* = u_{\psi dr}\mathrm{sgn}(\left|\psi_{dr}^* - \psi_{dr}\right|) \\ u_{\psi qr}^* = u_{\psi qr}\mathrm{sgn}(\left|\psi_{qr}^* - \psi_{qr}\right|) \end{cases} \tag{15}$$

It can be known from Fig. 2 that according to the relational expression (1) of the active and reactive power of the DFIG stator and the rotor flux linkage, the rotor flux component command values ψ_{qr}^* and ψ_{dr}^* can be calculated. Through the flux calculation part in real time, the flux feedback values ψ_{dr} and ψ_{qr} are calculated. The rotor magnetic chain sliding mode controller outputs adaptive control signals $u_{\psi dr}^*$ and $u_{\psi qr}^*$ of the inverter. When the power grid fails and disturbances occur, the adaptive control signal of the magnetic flux will be effective. Because the DFIG magnetic chain sliding mode controller is robust to external disturbances, the terminal voltage rise and low frequency oscillations caused by it are greatly weakened.

The DC system adaptive control links are shown in Figure 3. By collecting the AC bus frequency of the DC sending end and comparing it with the frequency setting value, the error signal obtained is sent to the PI regulator

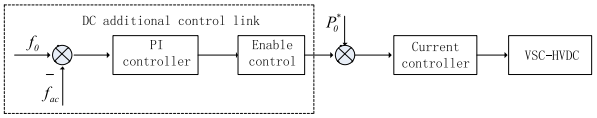

FIGURE 3. Block diagram of adaptive control of DC system.

through filtering and other links. When the system frequency fluctuates, the enabling link works, and the control is applied to the VSC-HVDC current controller, thereby changing the transmission power of the DC system and reducing or eliminating the instability of the transmission end of the ''wind and fire bundling'' DC delivery system. Balance the power and suppress the frequency fluctuation of the AC bus at the DC sending end.

IV. CASE STUDY

In order to verify the feasibility of the model in engineering applications, the single-machine DFIG control model was extended to a wind farm cluster control model, and a real-time simulation system of ''magnetic chain adaptive control'' based on RTDS was developed. The system experimental schematic is shown in Figure 4. Its main parameters are shown below.

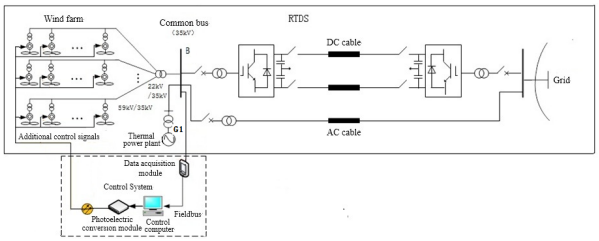

FIGURE 4. System experiment schematic diagram.

Doubly-fed wind turbine parameters: In the experiment, 4 equivalent wind turbines were used to simulate the wind farm, each with a rated capacity of 60MVA, a total of 240MVA. When the wind speed is 11m / s, the active output is 43MW per unit, for a total of 172MW. Stator resistance R_S is equal to 0.008Ω. Rotor resistance R_r is equal to 0.0019Ω (stator measurement). Stator inductance L_s is equal to 0.002H and L_r is equal to 0.0047H (stator measurement). Mutual sense L_m is equal to 0.00547H(stator measurement), and R is equal to 2.5kΩ.

Synchronous motor equivalent parameters: The synchronous machine has a rated capacity of 300MVA. Active output is 285MW. Rated frequency f_N is equal to 50Hz. Synchronous speed n_N is equal to 1800r/min. Stator resistance R_S is equal to 0.00076Ω. Rotor resistance R_r is equal to 0.000173Ω (stator measurement). Stator inductance L_s is equal to 0.012H and L_r is equal to 0.0047H (stator measurement). Mutual sense L_m is equal to 0.00375H (stator calculation value), and R is equal to 2.5kΩ.

The DC transmission power is 280MW. The rated voltage of the bus is 500kV and the rated frequency is 50Hz. The following test results are given as standard values (where the power base value is 540MVA).

During the experiment, the RTDS completes the real-time data acquisition of the wind farm and the system bus voltage, and transmits the data to the upper computer. After the DSP processes the data according to the set control algorithm, and the control signal passes through the optical fiber and the photoelectric conversion module. The specific control commands are assigned to the back-to-back converters of each DFIG in the wind farm, and finally a typical wind farm grid-connected feedback control system is formed, thereby realizing the real-time control of the wind farm grid-connected operation.

A. ADAPTIVE REACTIVE POWER CONTROL FOR WIND TURBINES

When t = 2s, set the ''wind-thermal bundled'' AC and DC delivery system bus B electrical remote ground fault, it's short-circuit time T is 0.2s. The output curve of each control quantity of the system is shown in Figure 5-9.

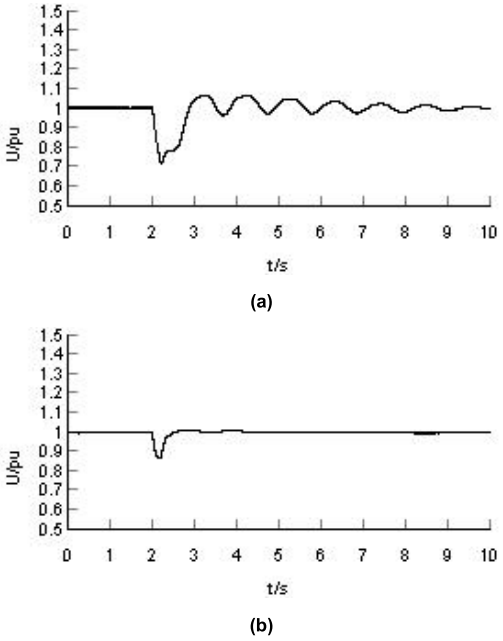

FIGURE 5. Sending voltage curve of bus B. (a) Sending voltage curve of bus B without adaptive control. (b) Sending voltage curve of bus B with adaptive control.

Fig. 5 shows the sending voltage curves of the bus bar B without adaptive control and with adaptive control. It can be seen from the figure that under the strategy without adaptive control, when the remote ground fault occurs, the voltage drop of the system bus B without adaptive control method is 0.3pu, as shown in Figure 5 (a). In the case of using adaptive control strategies, the voltage drop of the system bus B is only 0.15pu as shown in Figure 5 (b).

Fig. 6 shows the reactive output power curve of thermal power plant and wind farm without adaptive control and with adaptive control. It can be seen from the figure that under the strategy without adaptive control, when the remote

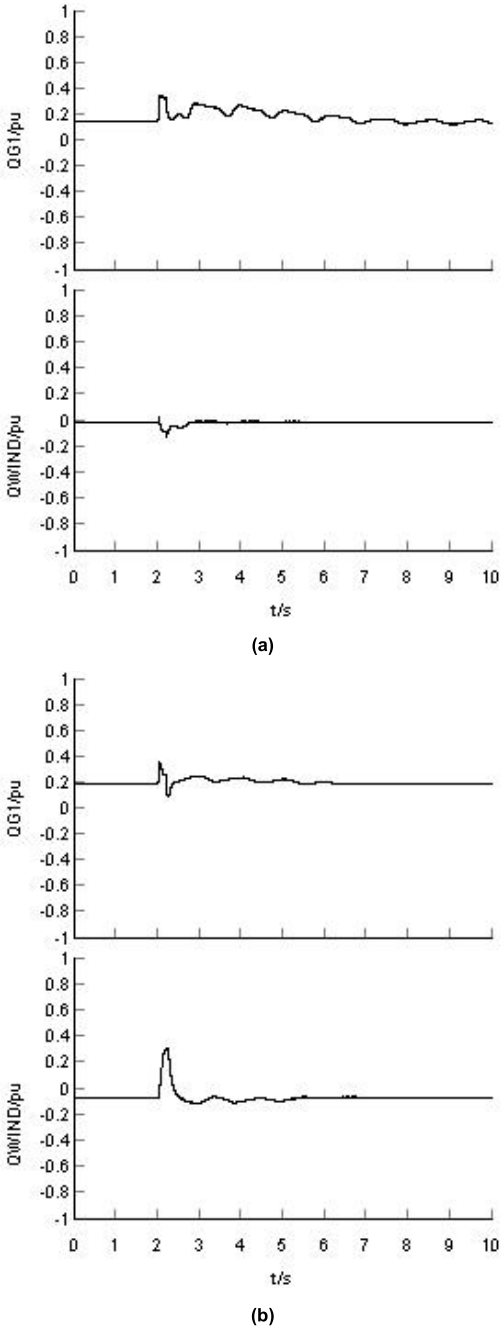

FIGURE 6. Reactive output power curve of thermal power plant and wind farm. (a) Reactive output power curve of thermal power plant and wind farm without adaptive control. (b) Reactive output power curve of thermal power plant 1 and wind farm with adaptive control.

ground fault occurs, only thermal power plants produce reactive power, while wind farms produce almost no change in reactive power, as shown in Figure 6 (a). In the case of using adaptive control strategies, thermal power plants and wind farms quickly issue reactive power at the same time, which effectively suppresses the voltage drop of bus B, as shown in Figure 6 (b).

Fig. 7 shows the DC transmission power curve of system without adaptive control and with adaptive control. It can be

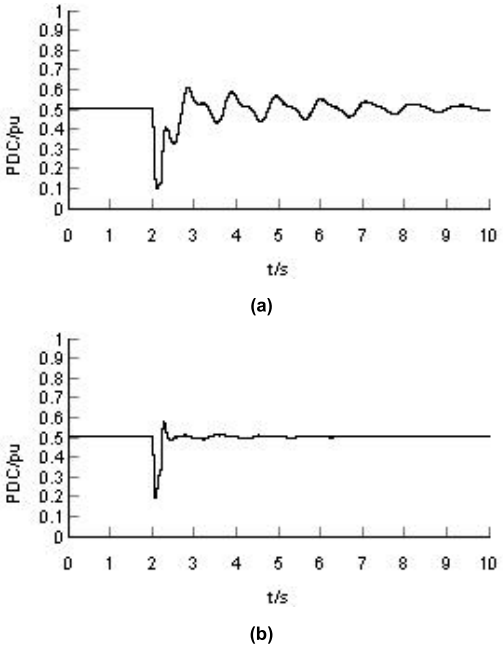

FIGURE 7. DC transmission power. (a) DC transmission power without adaptive control. (b) DC transmission power with adaptive control.

seen from the figure that under the strategy without adaptive control, when the remote ground fault occurs, the DC transmission power of the system drops to 0.1pu, as shown in Figure 7 (a). In the case of using adaptive control strategies, the DC transmission power drops to 0.2pu, as shown in Figure 7 (b).

Fig. 8 shows the active power output curve of thermal power plant and wind farm without adaptive control and with adaptive control. It can be seen from the figure that under the strategy without adaptive control, when the remote ground fault occurs, the active power of the thermal power plant oscillates violently and has a long recovery time, while the active power from the wind farm hardly changes, as shown in Figure 8 (a). In the case of using adaptive control strategies, although the active power of the thermal power plant also oscillated, the recovery time was short, and the active power from the wind farm hardly changed, as shown in Figure 8 (b).

B. ACTIVE POWER CONTROL OF WIND TURBINE

At t = 2s, set AC network line LAC failure of the ''wind and fire bundling'' AC and DC delivery system, and the disconnection duration T = 0.2s. Observe and record the output curve of each control amount of the system as shown in Figure 9 and Figure 12.

Fig. 9 shows the sending voltage curves of the bus bar B without adaptive control and with adaptive control. It can be seen from the figure that under the strategy without adaptive control, when the AC network line LAC fault occurs, the voltage of the system bus B oscillates with equal amplitude without adaptive control method, as shown in Figure 9 (a). In the case of using adaptive control strategies, after a small

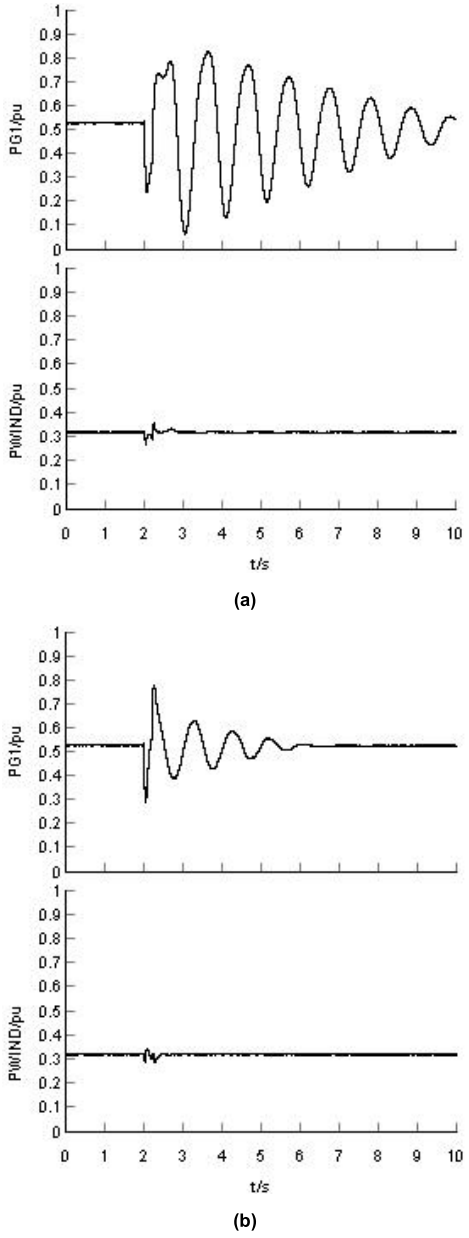

FIGURE 8. Active power output of thermal power plant and wind farm. (a) Active power output of thermal power plant 1 and wind farm without adaptive control. (b) Active power output of thermal power plant 1 and wind farm with adaptive control.

oscillation of bus voltage in the system, it returns to stability soon, as shown in Figure 9 (b).

Fig. 10 shows the sending frequency curves of the bus bar B without adaptive control and with adaptive control. It can be seen from the figure that under the strategy without adaptive control, when the when the AC network line LAC fault occurs, the frequency of the system bus B oscillates with equal amplitude without adaptive control method, as shown in Figure 10 (a). In the case of using adaptive control strategies, after a small oscillation of bus frequency in the system, it returns to stability soon, as shown in Figure 10 (b).

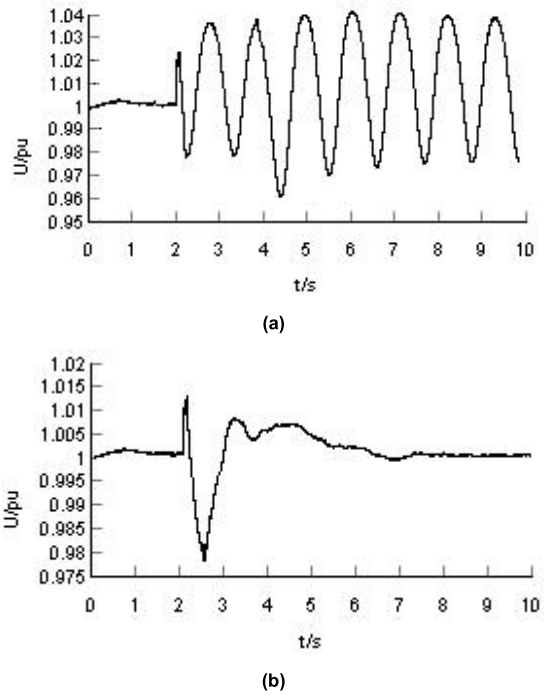

FIGURE 9. Sending voltage curve of bus B3. (a) Sending voltage curve of bus B3 without adaptive control. (b) Sending voltage curve of bus B3 with adaptive control.

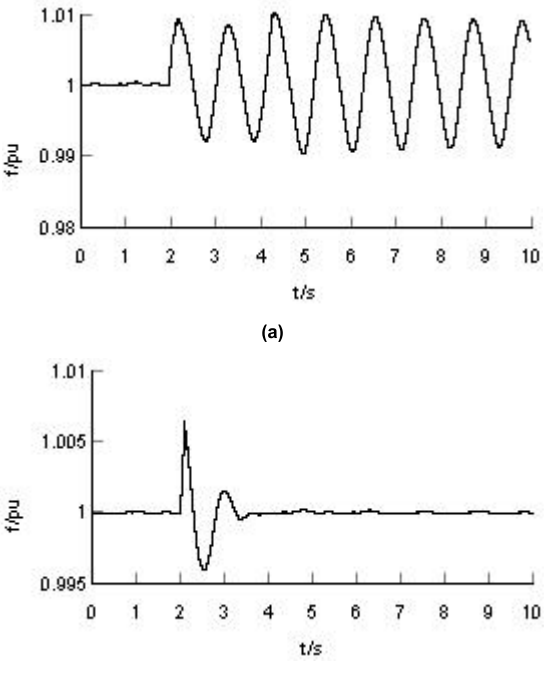

FIGURE 10. Sending end frequency. (a) Sending end frequency without adaptive control. (b) Sending end frequency with adaptive control.

Fig. 11 shows active power output curves of thermal power plant and wind farm. It can be seen from the figure that under the strategy without adaptive control, when the AC network line LAC fault occurs, the active power of the thermal power plant oscillates with equal amplitude without adaptive control

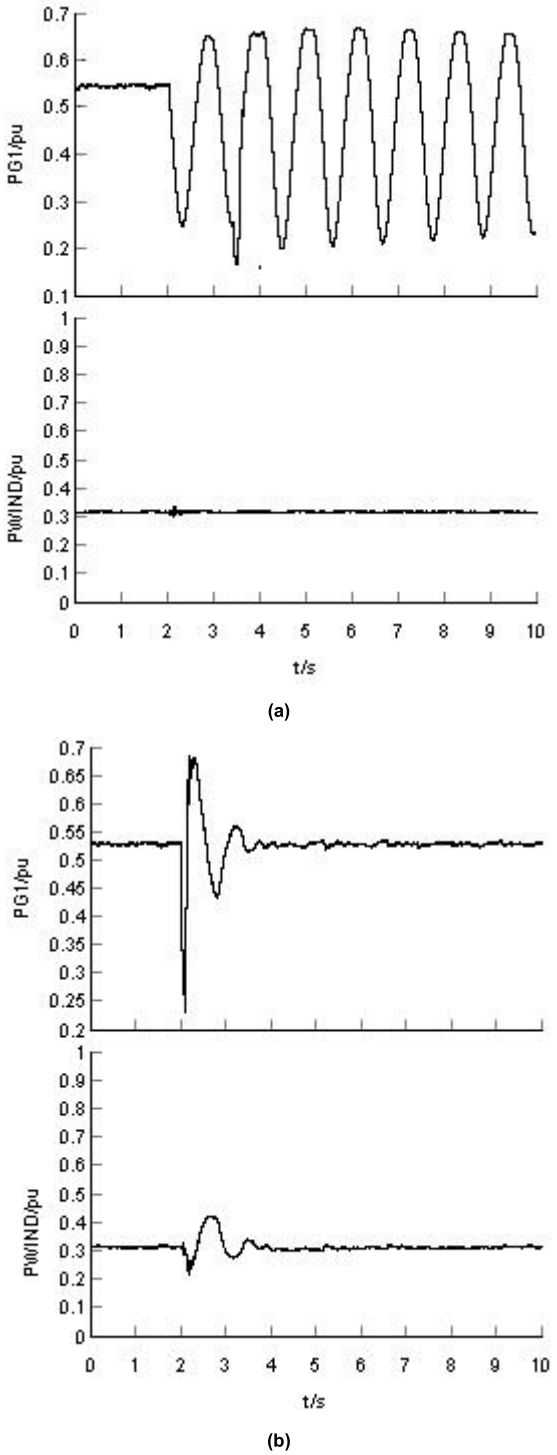

FIGURE 11. Active power output of thermal power plant and wind farm. (a) Active power output of thermal power plant 1 and wind farm without adaptive control. (b) Active power output of thermal power plant and wind farm with adaptive control.

method, while the active power of the wind farm hardly changes, as shown in Figure 11 (a). In the case of using adaptive control strategies, the active power of the thermal power plant and wind farm quickly issue reactive power at the same time, which effectively suppresses the frequency oscillation of system, as shown in Figure 11 (b).

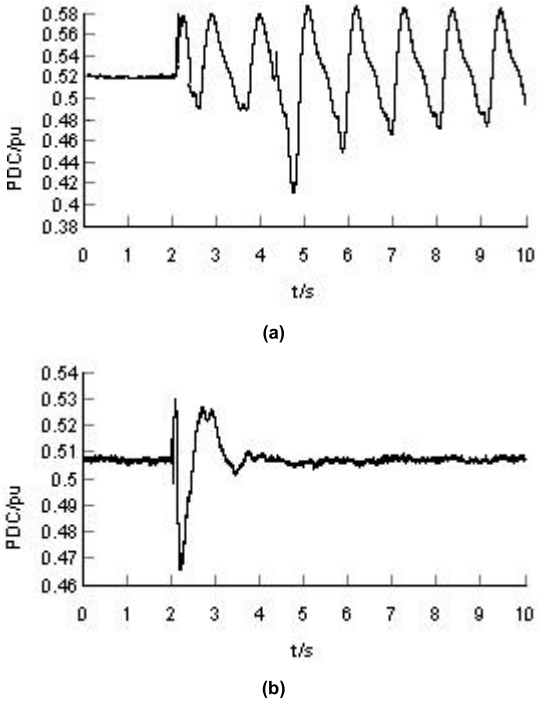

FIGURE 12. DC transmission power. (a) DC transmission power without adaptive control. (b) DC transmission power with adaptive control.

Fig. 12 shows the DC transmission power curves of system. It can be seen from the figure that under the strategy without adaptive control, when the AC network line LAC fault occurs, the DC transmission power oscillates with equal amplitude without adaptive control method, as shown in Figure 12 (a). In the case of using adaptive control strategies, the DC transmission power increases rapidly, which reduces the imbalance of instantaneous power and effectively suppresses the frequency oscillation of the system., as shown in Figure 12 (b).

V. CONCLUSION

Aiming at the transient stability of the voltage and frequency of the wind-fired AC / DC transmission system, this paper proposes an adaptive terminal sliding mode control algorithm based on the rotor flux linkage of the double-fed wind farm aimed at enhancing the transient stability of the voltage and frequency. Compared with the minute-level dispatch control during the current transmission system fault, this algorithm can realize the rapid adjustment of the active power and reactive power of the doubly-fed wind farm in milliseconds during the fault, which improves the transient characteristics of the transmission system. The experimental results show that, during the failure of the power system, the wind farm using the DFIG rotor flux linkage terminal sliding mode adaptive control strategy proposed in this paper can provide rapid support for active power and reactive power. This method can increase the damping of the system to effectively suppress the system voltage sag and low-frequency oscillation, and the control method will not negatively affect the fan and the system.

REFERENCES

[1] J. P. Prigol, "Control of active and reactive powers of a wind turbine equipped with DFIG to reduce the voltage violations in rural areas," in *Proc. Simposio Brasileiro de Sistemas Eletricos (SBSE)*, Niteroi, Brazil, May 2018, pp. 1–6.

[2] M. Edrah, O. Anaya-Lara, K. L. Lo, and A. Elansari, "Impact of DFIG based offshore wind farms connected through VSC-HVDC link on power system stability," in *Proc. 11th IET Int. Conf. AC DC Power Transmiss.*, Birmingham, U.K., 2015, pp. 1–7.

[3] L. Zeni, R. Eriksson, S. Goumalatsos, M. Altin, P. Sørensen, A. Hansen, P. Kjár, and B. Hesselba, "Power oscillation damping from VSC–HVDC connected offshore wind power plants," *IEEE Trans. Power Del.*, vol. 31, no. 2, pp. 829–838, Apr. 2016.

[4] Y. Meng, Q. Li, W. Hu, Z. Liu, and Q. Gong, "Research on transient stability of wind-thermal bundled system," in *Proc. 2nd IEEE Adv. Inf. Manage., Commun., Electron. Autom. Control Conf. (IMCEC)*, Xi'an, China, May 2018, pp. 2426–2430.

[5] H. W. Xiao, W. J. Du, Y. T. Song, Q. Wang, J. Ding, D. Z. Chen, H. F. Wang, and S. Q. Bu, "Wind-Thermal-Bundled power transmission by AC/DC system and coordinated control–A review," in *Proc. 12th IET Int. Conf. AC DC Power Transmiss. (ACDC)*, Beijing, China, 2016, pp. 1–6.

[6] Z. Sha, W. Liu, and S. Zheng, "Study on the stability of wind-thermal-bundled DC islanded sending end power system," in *Proc. China Int. Electr. Energy Conf. (CIEEC)*, Beijing, China, Oct. 2017, pp. 7–12.

[7] J. Ouyang, M. Li, T. Tang, D. Zheng, R. Yu, X. Zhang, and X. Xiong, "Advanced control strategy and its controllable area for doubly fed wind farm integrated into power systems with VSC-HVDC transmission under grid fault," *J. Eng.*, vol. 2017, no. 13, pp. 1170–1175, Jan. 2017.

[8] C. Yun, Z. Zhiqiang, C. Dezhi, G. Feng, Z. Shuang, S. Yunting, W. Yi, and L. Jian, "Studies on high-frequency generator tripping strategy for sending system of Wind-PV-thermal-Bundled power transmitted by HVDC," in *Proc. Int. Conf. Renew. Power Gener. (RPG)*, Beijing, China, 2015, pp. 1–6.

[9] P. He, S. A. Arefifar, C. Li, Y. Tao, and Q. Zhongjie, "Small-signal stability improvement of a DFIG integrated power system using PSS and SVC," in *Proc. IEEE Int. Conf. Electro/Information Technol. (EIT)*, Rochester, MI, USA, May 2018, pp. 0222–0227.

[10] J. Ouyang, T. Tang, J. Yao, and M. Li, "Active voltage control for DFIG-based wind farm integrated power system by coordinating active and reactive powers under wind speed variations," *IEEE Trans. Energy Convers.*, vol. 34, no. 3, pp. 1504–1511, Sep. 2019.

[11] Y. Shujun, G. Wanhua, H. Wenerda, X. Hongtao, and B. Erman, "Transient stability analysis of wind-thermal bundled system based on virtual inertia control," *J. Eng.*, vol. 2019, no. 16, pp. 862–866, Mar. 2019.

[12] R. Bai, Y. Zhang, F. Liang, Z. Shen, Y. Tang, K. Chang, and C. Li, "Research of generator-tripping strategy for wind-thermal-bundled power transmission system in emergency state," in *Proc. Asia–Pacific Power Energy Eng. Conf. (APPEEC)*, Xi'an, China, Oct. 2016, pp. 449–453.

[13] J. Liu, Q. Liu, R. Jiang, L. Zhang, and R. Wang, "Analysis of commutation failure of HVDC transmission system with wind farm," in *Proc. 2nd IEEE Conf. Energy Internet Energy Syst. Integr. (EI2)*, Beijing, China, Oct. 2018, pp. 1–6.

[14] Z. Li and F. Li, "Modeling and simulation of DFIG and a research on its equivalent method," *Renew. Energy Resour.*, vol. 31, no. 3, pp. 31–35, 2013.

[15] L. Sun, K. Liu, J. Hu, and Y. Hou, "Analysis and mitigation of electromechanical oscillations for DFIG wind turbines involved in fast frequency response," *IEEE Trans. Power Syst.*, vol. 34, no. 6, pp. 4547–4556, Nov. 2019.

[16] X. Xi, H. Geng, G. Yang, S. Li, and F. Gao, "Torsional oscillation damping control for DFIG-based wind farm participating in power system frequency regulation," *IEEE Trans. Ind. Appl.*, vol. 54, no. 4, pp. 3687–3701, Jul. 2018.

[17] C. Tu, J. Cao, L. He, and Y. Fang, "Combined active and reactive power control strategy to improve power system frequency stability with DFIGs," *J. Eng.*, vol. 2017, no. 13, pp. 2021–2025, Jan. 2017.

[18] S. S. Yu, T. K. Chau, T. Fernando, and H. H.-C. Iu, "An enhanced adaptive phasor power oscillation damping approach with latency compensation for modern power systems," *IEEE Trans. Power Syst.*, vol. 33, no. 4, pp. 4285–4296, Jul. 2018.

[19] K. Liao, Z. He, Y. Xu, G. Chen, Z. Y. Dong, and K. P. Wong, "A sliding mode based damping control of DFIG for interarea power oscillations," *IEEE Trans. Sustain. Energy*, vol. 8, no. 1, pp. 258–267, Jan. 2017.

XINYU LIU was born in Henan, China, in 1976. He received the master's and Ph.D. degrees from Zhengzhou University, China.

Since 2004, he has been working with the North China University of Water Resources and Electric Power. He is an Associate Professor and a Master Tutor with the North China University of Water Resources and Electric Power. He has authored two books.

CANBING LI, photograph and biography not available at the time of publication.

MOHAMMAD SHAHIDEHPOUR (Life Fellow, IEEE) is with the Department of Electrical and Computer Engineering, Illinois Institute of Technology, Chicago, IL, USA.

XINYAN LU was born in February 25, 1997. She is currently pursuing the master's degree with the North China University of Water Resources and Electric Power. Her main research interest includes the control strategy of converters with double-fed wind power grid-connected.

DI ZHANG, photograph and biography not available at the time of publication.